

Calibration of the isomer shift for the 14.4-keV transition in ^{57}Fe using the full-potential linearized augmented plane-wave method

U. D. Wdowik¹ and K. Ruebenbauer^{2,*}¹*Applied Computer Science Division, Institute of Technology, Pedagogical University, ulica Podchorążych 2, PL-30-084 Cracow, Poland*²*Mössbauer Spectroscopy Division, Institute of Physics, Pedagogical University, ulica Podchorążych 2, PL-30-084 Cracow, Poland*

(Received 7 May 2007; published 23 October 2007)

Full-potential linearized augmented plane-wave method has been used to calibrate isomer shift for the 14.4-keV resonant transition in ^{57}Fe . Augmented plane waves and local orbitals were used for the valence electrons. For the correlation and exchange potentials, a generalized gradient approximation has been adopted. Calculations have been performed for the following compounds: $\text{FeF}_2(P4_2/mnm)$, $\text{FeCl}_2(R\bar{3}m)$, $\text{FeBr}_2(P\bar{3}m1)$, $\text{FeI}_2(P\bar{3}m1)$, $\text{FeF}_3(R\bar{3}c)$, $\text{TiFe}(Pm\bar{3}m)$, and $\text{Fe}(Im\bar{3}m)$. Strong on-site Coulomb interactions in the Fe 3d shell of halides were taken into account by applying the Hubbard repulsion parameter U and the on-site exchange interaction constant J . The isomer shift calibration constant of $\alpha = -0.291$ a.u.³ mm s⁻¹ has been obtained. The nuclear quadrupole moment of the excited nuclear state involved was found to be $Q = +0.17$ b.

DOI: [10.1103/PhysRevB.76.155118](https://doi.org/10.1103/PhysRevB.76.155118)

PACS number(s): 76.80.+y, 71.10.-w, 71.15.Mb

I. INTRODUCTION

Mössbauer spectroscopy is one of the few methods being able to sample electric monopole interaction on the resonant nucleus via the hyperfine interactions. The sensitivity to the monopole interaction is due to the fact that hyperfine interactions are seen by this method in two different nuclear states. Hence, the solid-state effects influencing electron density on the resonant nucleus are sampled. The electric monopole interaction is observed via the isomer shift between two materials with resonant nuclei embedded in (Refs. 1 and 2). The above shift is, to good approximation, a product of the nuclear and electronic terms, thanks to the fact that the electron absolute charge density is small compared to the nuclear charge density within the nuclear volume.¹ It is important as well that the nuclear matter has very large stiffness and therefore remains practically unperturbed by the electronic shells of the atom and its surrounding. Therefore, one can approximate nuclear charge distribution by the homogeneously charged sphere, and one can assume that the electron density remains constant within such sphere. Under such circumstances, the isomer shift could be expressed as $\delta = \alpha(\rho_A - \rho_S)$. Symbols ρ_A and ρ_S stand for the electron density on the resonant nucleus in the absorber and source, respectively. Those are positive densities as they represent particle densities instead of the charge densities. The calibration constant α could be expressed as follows, provided that the change of the nuclear radius during the transition between two nuclear states is small compared in the absolute terms to the radius in either of these states: $\alpha = (Ze^2 \langle r^2 \rangle \delta R) / (\epsilon_0 E_0)$.^{1,2} The symbol Z stands for the atomic number, e denotes positive elementary charge, c stands for the speed of light in vacuum, $\langle r^2 \rangle$ represents mean squared charge radius of the nucleus (formally in the state with the more compact nuclear charge distribution), and δR denotes relative change of the nuclear charge radius in the transition. The last parameter is positive for the more compact charge distribution in the lower energy nuclear state (ground state), and negative for the opposite cases. The symbol ϵ_0 stands for the vacuum dielectric constant, while the symbol $E_0 > 0$ de-

notes transition energy between nuclear states involved to good approximation. Therefore, the calibration constant α is positive for nuclei expanding during transition from the ground to the excited state, and negative for nuclei contracting during such transition. Unfortunately, the calibration constant can neither be calculated nor measured reliably nowadays.

In principle, there are several experimental methods being able to measure this constant, such as the exact determination of the lifetime for highly converted transitions, determination of the respective conversion coefficients, and spectroscopy of the muonic atoms. Unfortunately, all of them require adoption of some nuclear models.²⁻⁶ On the other hand, the calibration constant could be determined in the almost nuclear model independent fashion calculating electron charge density in the resonant nucleus position.

Many calculations of the electron charge density have been performed in the past for various nuclei. Early attempts concentrated on the calculations for free atoms, ions, or molecules without taking into account solid-state effects.^{7,8} One has to bear in mind that the Mössbauer spectroscopy is impossible on the free molecules, and therefore, solid-state effects are to be taken into account. Recently, successful calculations taking into account solid-state effects have been performed for 23.88-keV transition in ^{119}Sn ,⁹ 37.15-keV in ^{121}Sb ,¹⁰ and partly for the 35.48-keV in ^{125}Te .¹¹ All these calculations were performed for nonmagnetic compounds. For the most commonly used 14.41-keV transition in ^{57}Fe , solid-state effects have been taken into account in the work by Eriksson and Svane.¹² They used linear muffin-tin orbitals in the atomic sphere approximation. The choice of compounds for the isomer shift calibration is also important, as one has to cover wide range of shifts, select simple and well characterized structures, and pay attention to the eventual disorder, i.e., one has to avoid nonstoichiometric systems or disordered alloys.

Therefore, we have attempted calibration of the isomer shift for the 14.41-keV transition in ^{57}Fe by means of the full-potential linearized augmented plane-wave method (FLAPW), which became the most accurate and reliable

method to include solid-state effects.¹³ The paper is organized as follows. Section II deals with the computational method and choice of iron compounds, and Sec. III discusses the results. The electric field gradient tensor (EFG) has been calculated as a by-product and compared with the available experimental data, where applicable. EFG is very sensitive to the proper choice of the basis set, and hence, it could be used to control the reliability of calculations.

II. COMPUTATIONAL METHOD, CHOICE OF COMPOUNDS, AND RESULTS

Calculations have been performed within density functional theory using the FLAPW and augmented plane wave plus local orbitals (APW+lo) methods as implemented in the WIEN2K code.^{14–16} Fully relativistic spin dependent approach was applied. The APW+lo extension was used for the valence electrons since it allows for the faster convergence at the same high level of accuracy as the LAPW+lo approach. In the FLAPW and APW+lo methods, the wave functions are expanded into spherical harmonics inside nonoverlapping atomic spheres centered on the atomic sites of radius R_{MT} and in plane waves in the remaining space of the unit cell (the so-called interstitial region between muffin-tin spheres). The radii R_{MT} used in the calculations fall in the range 2.0–2.85 a.u. for Fe and Ti and 1.64–2.85 a.u. for halide anions. The maximum angular momenta l for the expansion of the wave functions in the spherical harmonics inside the muffin-tin spheres were confined to $l_{max}=10$. The wave functions in the interstitial regions were expanded in plane waves with a cutoff of $K_{max}=8/\min(R_{MT})$, while the magnitude of the largest vector in the Fourier expansion of the charge density (G_{max}) was set to $16 \text{ Ry}^{1/2}$. The APW+lo basis for $l=0,1,2$ and the standard linearized augmented plane wave expansion for higher angular momenta l were used. States lying more than 7 Ry below the Fermi level were treated as the core states.

Iron compounds are difficult as they are magnetically ordered in the ground state except exotic spin states of iron. On the other hand, available computational methods deal with the ground state of the system. In order to cover wide range of shifts, it is desirable to choose high spin Fe^{2+} and high spin Fe^{3+} compounds as they form enough stoichiometric and well ordered structures. Additionally, one has to choose ground state bcc α -Fe as it is used as a reference point for the transition in question. Some perfectly ordered intermetallic compounds could be taken into account as well. Poorly defined structures should be avoided.

We have chosen the following set of Fe^{2+} high spin compounds: $\text{FeF}_2(P4_2/mnm)$,¹⁷ $\text{FeCl}_2(R\bar{3}m)$,¹⁸ $\text{FeBr}_2(P\bar{3}m1)$,¹⁹ and $\text{FeI}_2(P\bar{3}m1)$.²⁰ They are antiferromagnetic (AF) insulators in the ground state with relatively large EFG. Electric field gradient tensors are axially symmetric for all of these compounds except FeF_2 .²¹ All iron sites are crystallographically equivalent in these compounds, i.e., the primitive cell contains single iron atom. On the other hand, for the Fe^{3+} , high spin compound was chosen $\text{FeF}_3(R\bar{3}c)$, as it is also stoichiometric AF insulator with single iron atom per primi-

tive cell.²² It seems that this is the best characterized compound within this class with the collinear magnetic structure.²³ On the other hand, other compounds of this class may have noncollinear magnetic arrangements, and all of them have similar isomer shifts. Two metallic systems have been chosen: $\text{TiFe}(Pm\bar{3}m)$ (Ref. 24) and $\text{Fe}(Im\bar{3}m)$. Iron is ferromagnetically ordered. Magnetism of the above compounds is due to the iron moments aligned parallel (or antiparallel) to the $\langle 001 \rangle$ axis. On the other hand, $\text{TiFe}(Pm\bar{3}m)$ does not order magnetically and it has negligible magnetic moment on either iron or titanium. Our calculations were carried out with the experimental lattice constants (see Table I for details). The Brillouin zones of all insulators were sampled with a regular mesh containing from 50 to 70 irreducible k points, while for metallic structures, 286 irreducible k points were taken per Brillouin zone. The convergence of the quantities of interest with respect to the number of k points and the basis size, the latter determined by the $R_{MT}K_{max}$ criterion, was checked. At convergence, the integrated difference between the input and output charge densities was less than $5 \times 10^{-5} e/\text{a.u.}^3$. Number of radial mesh points was kept in all calculations as 781. For the correlation and exchange potentials, the generalized gradient approximation of Perdew *et al.* was used.²⁵ Strong on-site Coulomb interactions in the Fe $3d$ shell of halides were taken into account by applying the Hubbard repulsion parameter U and the on-site exchange interaction constant J in the form proposed by Anisimov *et al.*²⁶ The same parameters $U=5.50$ eV and $J=0.95$ eV were applied to all halide structures. These values are representative of those used for the Fe cation in other magnetic insulators.²⁷ Variation of the above parameters was tested for FeCl_2 . It was found that for $U=6.45$ eV and unchanged J , electron density increases by 0.018 a.u.^{-3} . On the other hand, setting $U=5.50$ eV and $J=0$ eV leads to the increase of the electron density by 0.064 a.u.^{-3} in comparison with the original value. Finally, setting $U=6.45$ eV and $J=0$ eV results in the decrease of the electron density by 0.003 a.u.^{-3} in comparison with the original value. These changes are small and do not affect the final results.

In order to calculate the electron contact densities on the Fe nucleus, the region near the nucleus having the radius of $R_0=4.987$ fm was applied. It corresponds to the radius of the homogeneously charged sphere, $R_0=1.123A^{1/3}+2.352A^{-1/3}-2.070A^{-1}$, with the mass number $A=57$.²⁸ For other elements, the same expression was used replacing the mass number of ^{57}Fe by the integer nearest to the average mass number of the respective element. The above expression is very similar to the Weizsäcker formula for the heavier nuclei.

Shifts S quoted in Table I were measured at 4.2 K for halides, while shift for metallic system TiFe is taken from the room temperature. Shift of bcc α -Fe is used as the reference shift, and therefore, it is temperature independent in the present context. They all include second order Doppler shift. Hence, the shift of the Table I is expressed as $S=\delta+\delta_D$. On the other hand, the second order Doppler term contributing to shift takes on the form $\delta_D=-\langle v^2 \rangle / (2c)$,¹ where the symbol $\langle v^2 \rangle$ stands for the mean squared velocity of the resonant atom. The above expression reduces to $\delta_D=-\langle E \rangle / (2mc)$ in

TABLE I. Crystallographic data, the differences in electron densities $\rho_A - \rho_{\text{Fe}}$, and relative experimental shifts $S_A - S_{\text{Fe}}$ are listed for compounds taken into account. Electron densities and shifts are shown versus metallic bcc α -Fe values. Lattice constants are given in Å, and angles are given in deg. Total electron density for bcc α -Fe amounts to $\rho_{\text{Fe}}(r=R_0) \approx \rho_{\text{Fe}} = 15\,322.046 \text{ a.u.}^{-3}$. The parameter ρ_{Fe} is determined within about 30% accuracy [see, for comparison, Hartree-Fock results (Ref. 7)] and it is the following function of the charge nuclear radius r (homogeneously charged sphere), $\rho_{\text{Fe}}(r) = \rho_0 + \rho_1 \exp(-r/R)$. It was found that $\rho_0 = 14\,660.7 \text{ a.u.}^{-3}$, $\rho_1 = 1775.6 \text{ a.u.}^{-3}$, and $R = 4.973 \text{ fm}$.

Compound	Crystallographic data	$\rho_A - \rho_{\text{Fe}}$ (a.u. ⁻³)	$S_A - S_{\text{Fe}}$ (mm/s)
FeF ₂ (P4 ₂ /mnm)	$a=4.83, c=3.36^a$	-5.073	+1.467 ^b
FeCl ₂ (R $\bar{3}m$)	$a=6.20, \alpha=33.55, x_{\text{Cl}}=0.2543^c$	-3.753	+1.093 ^d
FeBr ₂ (P $\bar{3}m1$)	$a=3.772, c=6.223, z_{\text{Br}}=0.25^e$	-4.156	+1.120 ^d
FeI ₂ (P $\bar{3}m1$)	$a=4.03, c=6.75, z_{\text{I}}=0.25^f$	-2.750	+1.044 ^d
FeF ₃ (R $\bar{3}c$)	$a=5.362, \alpha=58, x_{\text{F}}=0.836^g$	-1.739	+0.489 ^h
TiFe(Pm $\bar{3}m$)	$a=2.9760^i$	+0.441	-0.145 ^j
Fe(Im $\bar{3}m$)	$a=2.8311$	0	0

^aReference 17.

^bReference 21.

^cReference 18.

^dReference 29.

^eReference 19.

^fReference 20.

^gReference 22.

^hReference 30.

ⁱReference 24.

^jReference 31.

the vicinity of the ground state and for harmonic motion. Symbol $\langle E \rangle$ stands for the zero-point motion energy and m stands for the rest mass of the vibrating atom (formally in its ground nuclear state). For finite temperatures and within the phonon approximation, mean squared velocity satisfies the following condition:¹

$$\langle v^2 \rangle = \left(\frac{k_B}{2m} \right) \sum_{j=1}^3 \int_0^{+\infty} dx \left[\frac{\exp(x/T) + 1}{\exp(x/T) - 1} \right] D_j(x, T)$$

$$\text{with } \int_0^{+\infty} dx D_j(x, T) = 1. \quad (1)$$

Here, the symbol k_B stands for the Boltzmann constant, the index j enumerates three mutually orthogonal directions, and $D_j(x, T) \geq 0$ stands for the partial density of the phonon states (DOS) contributing to the resonant atom vibrations along the j th axis at temperature T . For low temperatures, one can assume that the above DOS is practically temperature independent. Mean squared velocity is also temperature independent at sufficiently low temperatures. On the other hand, mean squared velocity takes on the following simple form for sufficiently high temperature, $\langle v^2 \rangle = (3k_B T)/m$, according to the energy equipartition principle. A difference between absorber and source second order Doppler shifts, $S_D = \delta_D^{(A)} - \delta_D^{(S)}$, is accessible experimentally. Hence, this contribution to the total shift disappears in the first order approximation at high temperatures provided the source and absorber have nearly the same temperature. Term S_D could be observed for source and absorber kept both at low temperatures provided the zero-point motion energy is different for source and absorber, respectively. We have calculated $\delta_D^{(\text{Fe})}$ in the ground state by means of the *ab initio* calculated

Hellmann-Feynman forces.³² The latter forces were used to generate ground state DOS. It appears that this shift amounts to -0.11 mm/s . Owing to the fact that differences in the zero-point motion energies within compounds considered are about one order of magnitude smaller than the average zero-point motion energy, one can safely neglect corrections due to the second order Doppler shift. Usually, the room temperature total shift of α -Fe is used as the reference point. This shift differs from the ground state shift by the thermally generated second order Doppler shift and by the electron density change due to the thermal expansion. However, this is a constant shift and it has no influence on the calibration constant in the first order approximation. Generally, a thermal expansion is small between ground state and room temperature, and hence room temperature lattice constants (including angles) and atomic positions could be safely adopted provided there is no structural phase transition within the above temperature range. Data point for room temperature TiFe is still on the straight line (see Fig. 1), indicating that the total shift between ground state and room temperature is sufficiently small for this compound. Figure 1 shows experimental shift plotted versus difference in electron density for compounds used in calibration.

A resonant nuclear transition occurs here between ground nuclear state with spin and parity $I_g^{(\pi)} = \frac{1}{2}(-)$ and the first excited state with the spin and parity $I_e^{(\pi)} = \frac{3}{2}(-)$. It is almost pure $M1$ transition.¹ Hence, the ground state remains doubly degenerated for nonvanishing EFG, while the excited state splits into Kramers doublet provided magnetic interactions are absent or very weak. Under such circumstances and for the microscopically random absorber, one can observe solely splitting of the excited state expressed as $\Delta = 6|A_Q| \sqrt{1 + \eta^2}/3$.¹ The quadrupole coupling constant is expressed to high accuracy here as A_Q

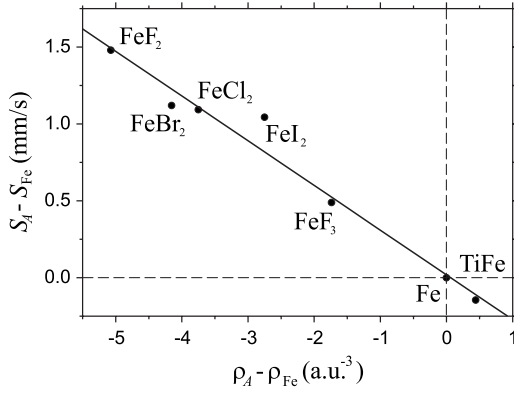


FIG. 1. Relative experimental shift plotted versus difference in electron density for various compounds.

$=(ecQV_{zz})/[4I_e(2I_e-1)E_0]$, while the asymmetry parameter is expressed as $\eta=(V_{xx}-V_{yy})/V_{zz}$. Symbol Q stands for the spectroscopic nuclear electric quadrupole moment in the first excited state, while symbols V_{xx} , V_{yy} , and V_{zz} denote principal components of the electric field gradient tensor on the nucleus. The following convention is applied $|V_{xx}| \leq |V_{yy}| \leq |V_{zz}|$, and therefore, the asymmetry parameter satisfies the condition $0 \leq \eta \leq 1$. For axially symmetric EFG, one obtains $\eta=0$. One has to remember that the EFG tensor is always symmetric and traceless. Hence, the following relationship is always obeyed: $V_{xx}+V_{yy}+V_{zz} \equiv 0$. For the magnetically ordered state, a hyperfine magnetic field could appear, and therefore more information could be gained. Namely, the excited state hyperfine nonscalar part of the Hamiltonian takes on the following form in the principal axes of EFG:¹

$$\mathbf{H}_e = A_Q[3\mathbf{I}_z^2 - \mathbf{I}^2 + \eta(\mathbf{I}_x^2 - \mathbf{I}_y^2)] - a[\mathbf{I}_z \cos \beta + \sin \beta(\mathbf{I}_x \cos \gamma + \mathbf{I}_y \sin \gamma)]. \quad (2)$$

Symbols \mathbf{I}_x , \mathbf{I}_y , and \mathbf{I}_z denote respective (excited state) nuclear spin projection operators on the orthogonal principal axes of EFG, while \mathbf{I} stands for the total (excited state) nuclear spin operator. Magnetic dipole coupling constant is well approximated by the form $a=(cg_e\mu_N B)/E_0$. Symbol g_e stands for the effective nuclear gyromagnetic factor in the nuclear state under consideration, μ_N denotes nuclear magneton, and B stands for the absolute value of the magnetic hyperfine field on the nucleus. Angles β and γ denote polar and azimuthal angles of the hyperfine field in the principal axes of EFG, respectively. The Hamiltonian described by Eq. (2) allows determination of the sign of the quadrupole coupling constant and asymmetry parameter under favorable conditions. Results for the EFG calculations are summarized in Table II for the compounds with nonvanishing EFG. Electric field gradient vanishes for the local symmetry being cubic. Hyperfine fields are very small in the ground state of divalent halides except FeF_2 due to the cancellation of the contact, orbital, and dipolar contributions.³³ On the other hand, the quadrupole interaction is very small for FeF_3 .³⁰ Therefore, the sign of the quadrupole coupling constant is determined unambiguously solely for the nonaxial case of FeF_2 . The spin-orbit coupling (SO) has been neglected in

TABLE II. Calculated and experimental data are shown for the EFG in various compounds. Hyperfine contact field is shown for divalent fluoride, where the SO and dipolar terms are relatively small. Experimental quadrupole splitting Δ_{exp} is shown with the sign of the coupling constant for the unambiguous case of FeF_2 .

Compound	V_{zz} (10^{21} V/m ²)	η	Δ_{exp} (mm/s)	η_{exp}	B (T)	B_{exp} (T)
$\text{FeF}_2(P4_2/mmm)$	+15.79	0.3	+2.85 ^a	0.4 ^a	36.8	32.9 ^a
$\text{FeCl}_2(R\bar{3}m)$	-7.08	0.0	1.21 ^b			
$\text{FeBr}_2(P\bar{3}m1)$	-6.64	0.0	1.132 ^b			
$\text{FeI}_2(P\bar{3}m1)$	+4.36	0.0	0.962 ^b			
$\text{FeF}_3(R\bar{3}c)$	-0.28	0.0	0.044 ^c			

^aReference 21.

^bReference 29.

^cReference 30.

present calculations as it has negligible effect on the charge distribution. Hence, the hyperfine fields for divalent halides have not been calculated except for divalent fluoride, where the dominant contribution to the hyperfine field is due to the contact term. It appears that for this compound, V_{xx} is aligned with the hyperfine field, the latter being aligned with the $\langle 001 \rangle$ axis. Hence, the angles of Eq. (2) take on the following values for this compound: $\beta=90^\circ$ and $\gamma=0^\circ$. The SO contribution to the iron hyperfine field in FeF_3 is also quite significant. For the metallic iron, we have obtained hyperfine contact field of 34.4 T in comparison with the experimental field at room temperature of 33.0 T.

Figure 2 shows experimental quadrupole splitting (absolute value of the splitting) versus calculated effective electric field gradient $|V_{zz}|\sqrt{1+\eta^2/3}$.

III. DISCUSSION

Linear regression fit to the data of Fig. 1 gives the isomer shift calibration constant of $\alpha=-0.291(14)$ a.u.³ mm s⁻¹. Upon having excluded FeI_2 ,

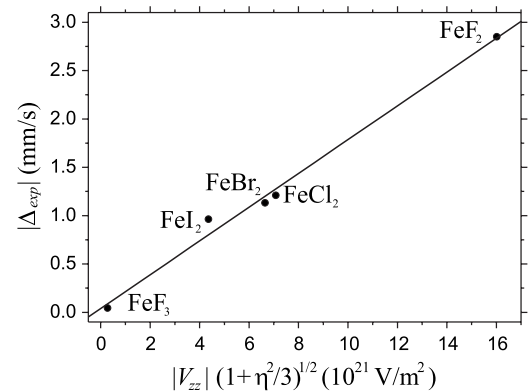


FIG. 2. Experimental quadrupole splitting is plotted versus calculated effective electric field gradient.

one obtains $\alpha = -0.285(5)$ a.u.³ mm s⁻¹, while exclusion of FeBr₂, results in $\alpha = -0.304(15)$ a.u.³ mm s⁻¹. Exclusion of both of the above compounds yields $\alpha = -0.291(2)$ a.u.³ mm s⁻¹. Similar linear regression fit to the data of Fig. 2 gives the nuclear quadrupole moment of $Q = +0.17(1)$ b. Errors quoted above are solely due to the errors of linear regression. Positive sign of the quadrupole moment is determined from the FeF₂ data. Actual errors for both of the above parameters (α and Q) are, in fact, larger than linear regression errors and they are about 10% due to the various approximations used and uncertainty of the experimental data.

Previous values for the isomer shift calibration constant determined by means of the electron density calculations varied from $\alpha = -0.11$ a.u.³ mm s⁻¹ (Ref. 34) to $\alpha = -0.62$ a.u.³ mm s⁻¹ (Ref. 35) for the transition considered here. Our value is very close to the value obtained by Trautwein *et al.*³⁶ All of the above calculations have been performed neglecting solid-state effects. Ericksson and Svane¹² obtained $\alpha = -0.22$ a.u.³ mm s⁻¹ using a method similar to the method used by us with the solid-state effects accounted for. Similar calculations albeit without determination of the

calibration constant and for nonrelativistic electrons have been performed by Akai *et al.*³⁷ Detailed review of the previous attempts aimed at the determination of the calibration constant for the 14.41-keV transition in ⁵⁷Fe by means of the electron density calculation is given in Ref. 7.

The electric quadrupole moment of the first excited state of ⁵⁷Fe has been estimated in the early days of the Mössbauer spectroscopy as lying in between $Q = +0.15$ b and $Q = +0.28$ b.³⁸ Calculations performed later on and some comparisons with the nuclear models suggested $Q = +0.082$ b.^{39,40} However, detailed calculations performed by Dufek *et al.*³⁸ with the solid-state effects accounted for lead to $Q = +0.16$ b, in excellent agreement with our value.

ACKNOWLEDGMENTS

Jakub Bielecki, Institute of Physics, Pedagogical University, Cracow, Poland is warmly thanked for supervising the execution of some computer jobs. This work was partly supported by Ministry of Science, Poland, under the Grant No 3T11F03129.

*Corresponding author; sfrueben@cyf-kr.edu.pl

¹N. N. Greenwood and T. C. Gibb, *Mössbauer Spectroscopy* (Chapman and Hall, London, 1971).

²*Mössbauer Isomer Shifts*, edited by G. K. Shenoy and F. E. Wagner (North-Holland, Amsterdam, 1978).

³J. P. Bocquet, Y. Y. Chu, O. C. Kistner, M. L. Perlman, and G. T. Emery, *Phys. Rev. Lett.* **17**, 809 (1966).

⁴G. T. Emery and M. L. Perlman, *Phys. Rev. B* **1**, 3885 (1970).

⁵P. Roggwiller and W. Kündig, *Phys. Rev. B* **11**, 4179 (1975).

⁶A. Meykens, R. Coussemont, J. Ladrière, M. Cogneau, M. Bogé, P. Auric, R. Bouchez, A. Benabed, and J. Godard, *Phys. Rev. B* **21**, 3816 (1980).

⁷K. J. Duff, *Phys. Rev. B* **9**, 66 (1974).

⁸W. C. Niewpoort, D. Post, and P. Th. van Duijnen, *Phys. Rev. B* **17**, 91 (1978).

⁹A. Svane, N. E. Christensen, C. O. Rodriguez, and M. Methfessel, *Phys. Rev. B* **55**, 12572 (1997).

¹⁰A. Svane, *Phys. Rev. B* **68**, 064422 (2003).

¹¹P. E. Lippens, C. J. Jumas, and J. Olivier-Fourcade, *Hyperfine Interact.* **141/142**, 303 (2002).

¹²O. Eriksson and A. Svane, *J. Phys.: Condens. Matter* **1**, 1589 (1989).

¹³P. Blaha, K. Schwarz, P. I. Sorantin, and S. B. Trickey, *Comput. Phys. Commun.* **59**, 399 (1990).

¹⁴E. Sjöstedt, L. Nordström, and D. J. Singh, *Solid State Commun.* **114**, 15 (2000).

¹⁵G. K. H. Madsen, P. Blaha, K. Schwarz, E. Sjöstedt, and L. Nordström, *Phys. Rev. B* **64**, 195134 (2001).

¹⁶K. Schwarz, P. Blaha, and G. K. H. Madsen, *Comput. Phys. Commun.* **147**, 71 (2002); P. Blaha, K. Schwarz, G. K. H. Madsen, K. Kvasnicka, and J. Luitz, computer code WIEN2K, Vienna University of Technology, Vienna, 2001.

¹⁷R. A. Erickson, *Phys. Rev.* **90**, 779 (1953).

¹⁸M. K. Wilkinson, *J. Appl. Phys.* **30**, S278 (1959).

¹⁹M. K. Wilkinson, J. W. Cable, E. O. Wollan, and W. C. Koehler, *Phys. Rev.* **113**, 497 (1959).

²⁰J. Gelard, A. R. Fert, P. Meriel, and Y. Allain, *Solid State Commun.* **14**, 187 (1974).

²¹G. K. Wertheim and D. N. E. Buchanan, *Phys. Rev.* **161**, 478 (1967).

²²F. R. Morral, *J. Met.* **10**, 662 (1958).

²³E. O. Wollan, H. R. Child, W. C. Koehler, and M. K. Wilkinson, *Phys. Rev.* **112**, 1132 (1958).

²⁴D. A. Papaconstantopoulos, *Phys. Rev. B* **11**, 4801 (1975).

²⁵J. P. Perdew, K. Burke, and M. Ernzerhof, *Phys. Rev. Lett.* **77**, 3865 (1996).

²⁶V. I. Anisimov, I. V. Solovyev, M. A. Korotin, M. T. Czyzyk, and G. A. Sawatzky, *Phys. Rev. B* **48**, 16929 (1993).

²⁷I. I. Mazin and V. I. Anisimov, *Phys. Rev. B* **55**, 12822 (1997); J. Kuneš, H. Rosner, Deepa Kasinathan, C. O. Rodriguez, and W. E. Pickett, *ibid.* **68**, 115101 (2003).

²⁸L. R. B. Elton, *Nuclear Sizes* (Oxford University Press, Oxford, 1961).

²⁹E. Pfletschinger, *Z. Phys.* **209**, 119 (1968).

³⁰G. K. Wertheim, H. J. Guggenheim, and D. N. E. Buchanan, *Phys. Rev.* **169**, 465 (1968).

³¹E. V. Mielczarek and W. P. Winfree, *Phys. Rev. B* **11**, 1026 (1975).

³²K. Parlinski, Z.-Q. Li, and Y. Kawazoe, *Phys. Rev. Lett.* **78**, 4063 (1997); K. Parlinski, software PHONON, Cracow, 2005.

³³D. J. Simkin, *Phys. Rev.* **177**, 1008 (1969).

³⁴E. Simanek and Z. Sroubek, *Phys. Rev.* **163**, 275 (1967).

³⁵R. A. Uher and R. A. Sorensen, *Nucl. Phys.* **86**, 1 (1966).

³⁶A. Trautwein, J. R. Regnard, Frank E. Harris, and Y. Maeda, *Phys. Rev. B* **7**, 947 (1973).

³⁷H. Akai, S. Blügel, R. Zeller, and P. H. Dederichs, Phys. Rev. Lett. **56**, 2407 (1986).

³⁸P. Dufek, P. Blaha, and K. Schwarz, Phys. Rev. Lett. **75**, 3545 (1995).

³⁹K. J. Duff, K. C. Mishra, and T. P. Das, Phys. Rev. Lett. **46**, 1611 (1981).

⁴⁰S. Vajda, G. D. Sprouse, M. H. Rafailovich, and J. W. Noe, Phys. Rev. Lett. **47**, 1230 (1981).